Mode decomposed passivity-based speed control of DC drive with bidirectional Zeta-SEPIC DC-DC converter for light electric vehicles

Rostyslav-Ivan V. Kuzyk[1]
ORCID: https://orcid.org/0000-0002-6483-2223; rostyslav-ivan.v.kuzyk@lpnu.ua
Ihor Z. Shchur[1]
ORCID: https://orcid.org/0000-0001-7346-1463; ihor.z.shchur@lpnu.ua. Scopus Author ID: 36348908300
[1] Lviv Polytechnic National University, 12, S. Bandera Str. Lviv, 79013, Ukraine

ABSTRACT

Currently, light electric vehicles are rapidly developing in various kinds. To power these vehicles with batteries, the simplest electric drive system is a DC motor controlled by a DC-DC converter. This work utilizes a bidirectional Zeta-SEPIC DC-DC converter with an integrated DC motor. This implementation enables control of motor speed and torque in traction and regenerative braking modes. Additionally, it allows for the use of a lower voltage battery compared to the motor's rated voltage, reducing battery weight and increasing safety. In this work, a decomposition approach is applied. Two separate port-controlled Hamiltonian subsystems are obtained to adjust the motor angular velocity in the traction (Zeta) and braking (SEPIC) modes of the DC-DC converter. The Passivity-Based Control (PBC) method is used to synthesize the drive control subsystems in these modes. This method is based on the energy laws of processes in systems and provides asymptotic stability of nonlinear systems, in this case, two fourth-order subsystems for speed control. Two third-order current control subsystems synthesized by the PBC were used to limit the motor current at a given level. The synthesis resulted in sets of possible structures of control influence formers (CIFs) for all PBC subsystems using Zeta and SEPIC DC-DC converters. The study analyzed the operation of the obtained structures of the CIFs, selected the most effective ones, and determined the laws of adaptation of their parameters to the value of the motor angular velocity through computer simulation in Matlab/Simulink. The results of the simulation showed that the drive operated well in both static and dynamic modes.

Keywords: Light electric vehicle; Zeta DC-DC converter; SEPIC DC-DC converter; DC drive; passivity-based control (PBC); port-controlled Hamiltonian (PCH) system; Interconnection and Damping Assignment (IDA)

INTRODUCTION

In recent years, the automotive market has undergone rapid changes. Traditional vehicles with internal combustion engines are being replaced by autonomous electric vehicles (EVs) of various shapes and capacities [1]. The main reason for this shift is the need to address the environmental problems caused by the massive use of cars in large cities. This shift is also facilitated by the improvement of rechargeable batteries, particularly the lithium group [2]. A new group of EVs, called light EVs (LEV), has emerged. LEVs come in various shapes and serve multiple purposes, particularly in urban and suburban areas [3]. This group includes personal LEVs for micromobility, such as e-bikes, kick e-scooters, and electric two-wheelers, as well as the L7e-C category of LEVs with a rated power up to 15 kW and a maximum speed up to 90 km/h [4, 5].

To form on-board buses of LEVs, as a rule, Li-ion batteries with an energy capacity of 5-15 kWh of low voltage and high specific capacity are used. That simultaneously guarantees the safety of operation and provides the necessary range of LEVs [4]. To regulate the electromagnetic torque and speed of the drive motor, a DC-DC converter is required for powering a brush DC motor or a brushless DC motor (BLDC), which is controlled only by DC voltage. The DC-DC converter output voltage needs to be adjusted from zero voltage at motor start to a nominal motor voltage high enough to provide maximum LEV speed. To achieve this, the DC-DC converter must be of the buck/boost type. The main topologies that implement this function are classic buck/boost, Cuk, Zeta, and Single-Ended Primary-Inductance Converter (SEPIC) [6, 7], [9, 10], [11]. Among these types, the last two are distinguished from the others by the presence of a common negative bus for the input and output voltages of the converter. This feature allows the output voltage to maintain the same polarity as the power source.

To preserve the kinetic energy of motion in the battery during LEV braking, it is necessary to implement the regenerative braking mode of the motor

using the bidirectional type of DC-DC converter [10,11], [12]. Studies have shown that combining Zeta and SEPIC topologies can result in an efficient bidirectional buck/boost DC-DC converter [13, 14]. The converter uses two power switches with free-wheeling diodes, as shown in Fig. 1a. The Zeta DC-DC converter operates in the traction mode and controls by a PWM signal applied to the S1 switch. When S1 is closed, the reactive currents of the both chokes L1 and L2 flow through the diode of the S2 switch. In regenerative braking mode, the SEPIC DC-DC converter operates, in reverse, by the PWM controlled S2 switch, and the reactive currents of the chokes flow through the freewheeling diode of the S1 switch.

Fig. 1b shows the scheme of the LEV electric drive system under study. The bidirectional Zeta-SEPIC DC-DC converter, which integrates a DC motor M, differs from the one shown in Fig. 1a. In this case, the motor armature winding serves as the output choke L2, and the back-EMF of the motor E_M performs the function of the output capacitor C2. A similar solution was used in previous studies [15, 16] to implement a BLDC-based electric drive system. The low-voltage battery B is modeled by the EMF E_B and internal series resistance R_B. The circuit also considers the internal resistance R_1 of the choke L1. Fig. 1b shows also the electromagnetic motor torque $T_e = k_e i_a$, where the motor constant is represented by the symbol $k_e = E_M/\omega$, ω is the angular velocity of the motor, and the load torque applied to the shaft is denoted by T_L.
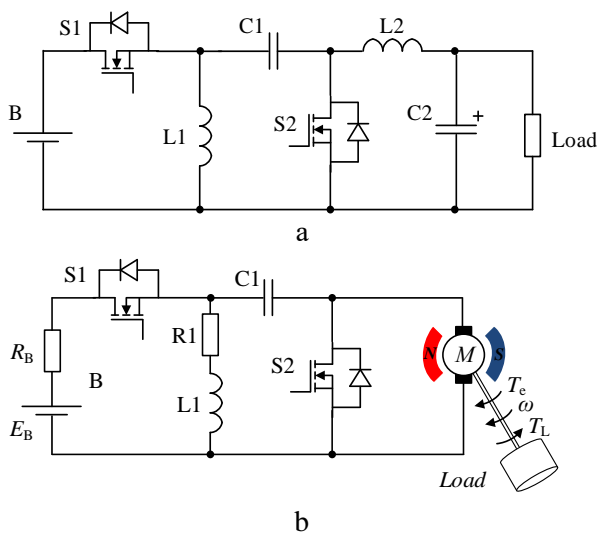

Fig. 1. **Scheme of the bidirectional Zeta-SEPIC DC-DC converter (a) and the design scheme of power part of the DC drive system based on it (b)**
Source: **compiled by the authors**

LITERATURE REVIEW

The Zeta and SEPIC DC-DC converters utilize four passive elements – two chokes L1 and L2 and two capacitors C1 and C2 (see Fig. 1a). These elements respectively store the energy of the magnetic and electrostatic fields. The mathematical models that describe the dynamics of these converters are systems of fourth-order differential equations [12, 14], [16]. The synthesis of an electric drive control system using Zeta and SEPIC DC-DC converters is significantly complicated due to the nonlinear transfer functions that describe all DC-DC converters and their non-minimally phase characteristics in voltage boost mode. This presents the challenge of ensuring both system stability and control quality. Numerous studies have been conducted to address these issues using modern control theory methods. They include multi-loop control systems with PI, PID, or fractional order controllers, adaptive control, intelligent methods such as fuzzy logic and genetic algorithms, and model predictive control [17, 18], [19, 20], [21]. A promising new area of research for synthesizing control systems for complex nonlinear objects with multiple inputs and outputs is the Passivity-Based Control (PBC) method [22, 23], [24]. This method offers the advantage of providing a clear understanding of the physical processes involved in forming control influences and ensuring the asymptotic stability of the controlled nonlinear system.

To synthesize a system using the PBC method, the control object should be viewed as a port-controlled Hamiltonian (PCH) system, which takes the following form [23, 24], [25]:

$$\dot{\mathbf{x}}(t) = [\mathbf{J}(\mathbf{x}) - \mathbf{R}(\mathbf{x})]\nabla H(\mathbf{x}) + \mathbf{G}(\mathbf{x})\mathbf{u}(t), \qquad (1)$$

where $\mathbf{x}(t)$ is the vector of state variables, $\mathbf{J}(\mathbf{x})$ is the asymmetric interconnection matrix, $\mathbf{R}(\mathbf{x})$ is the semi-definite symmetric damping matrix, $H(\mathbf{x})$ is the system energy storage function (Hamiltonian function), $\mathbf{G}(\mathbf{x})$ is the input port matrix, and $\mathbf{u}(t)$ is the vector of system input variables.

The Interconnection and Damping Assignment (IDA) method [22, 23], [24] is the primary means of structurally synthesizing PBC systems. The IDA-PBC method aims to obtain control influence formers (CIF) structures on the system that ensure the movement of the closed-loop system to a given desired equilibrium point. At this point, the Hamiltonian H_d, takes the minimum value.

The vector-matrix equation below describes the dynamics of the closed-loop system:

$$\dot{\tilde{\mathbf{x}}}(t) = [\mathbf{J}_d(\tilde{\mathbf{x}}) - \mathbf{R}_d(\tilde{\mathbf{x}})]\nabla H_d(\tilde{\mathbf{x}}), \qquad (2)$$

where $H_d(\tilde{\mathbf{x}}) = 0.5\,\tilde{\mathbf{x}}^T\mathbf{D}\tilde{\mathbf{x}}$, $\tilde{\mathbf{x}} = \mathbf{x} - \overline{\mathbf{x}}$ is the new vector of state variables whose elements are the errors between the coordinates given by the equilibrium point vector $\overline{\mathbf{x}}$ and the actual values of the corresponding coordinates given by the state vector $\mathbf{x}$ and $\mathbf{D}$ is the diagonal inertia matrix.

The desired values of the interconnections and damping of the system are achieved by introducing additional interconnections and damping, which can be written as:

$$\mathbf{J_d} = \mathbf{J} + \mathbf{J_a}\,, \qquad (3)$$

$$\mathbf{R_d} = \mathbf{R} + \mathbf{R_a}\,, \qquad (4)$$

where $\mathbf{J_a}$ and $\mathbf{R_a}$ are the matrices of interconnections and damping, respectively, which form the control influences in the system, i.e. are actually the control system.

The goal of synthesizing asymptotically stable PBC systems is to determine the appropriate structures of $\mathbf{J_a}$ and $\mathbf{R_a}$ that ensure the identity of the expressions (1) and (2). The authors have developed their own methodology to accomplish this task. It involves the symbolic solution of the vector-matrix equation in the MathCad environment [16, 23], [24].

In our previous study [25], satisfactory results were obtained in the synthesis of the output voltage control system of the alone bidirectional Zeta-SEPIC DC-DC converter operating with an R-L-E load using the IDA-PBC method. In order to obtain the same quality indicators of the system operation in both static and dynamic mode, control effects were adapted to the value of the converter output voltage.

THE PURPOSE OF THE ARTICLE

The objective of this work is to synthesize passive control systems using the IDA-PBC method for the traction and braking modes of the studied DC electric drive system with a DC motor integrated with a bidirectional Zeta-SEPIC DC-DC converter. Taking into account the different structures of the control object in traction and braking modes, a decomposition approach was applied [25] and the general mathematical model was divided into two subsystems for each mode. Each subsystem was represented as a separate PCH system for Zeta and SEPIC DC-DC converters, respectively, in the traction and braking modes of the LEV electric drive.

To achieve this goal, it is necessary to solve the following tasks:

• to develop mathematical models of the studied subsystems in the form of PCH systems;

• to create programs in Mathcad for symbolic solution of systems of matrix equations and to obtain

of the possible CIF structures, which will be accessible for practical implementation;

• to develop a computer model of the studied LEV electric drive in the MATLAB/Simulink environment;

• to investigate the effectiveness of individual elements of interconnection and damping, which are part of the obtained CIF structures, on the operation of the studied electric drive system and to select the most effective CIF structures for each of the drive operation modes;

• to perform a computer simulation study of the operation of the subsystems with the obtained CIFs structures and to adjust their parameters in order to ensure the same static and dynamic performance of the drive over the whole range of its speed control.

DESCRIPTION OF THE STUDIED SYSTEM WORK AND ITS MATHEMATICAL MODELING

The DC drive in the traction mode with the Zeta DC-DC converter

When the DC motor operates in traction mode, its power is provided by the Zeta DC-DC converter, which transfers energy from the battery B to the electric motor M. The switching is performed by the S1 switch.

When the S1 switch is turned on (see Fig. 2a), two parallel circuits are formed for the current from the battery (shown by red lines). In the first small circuit, the current flows through the choke L1, charging it with part of the energy. The second large circuit is formed by the capacitor C1, which is closed by the motor armature winding.

When the switch S1 is turned off, the battery is disconnected from the common circuit (Fig. 2b), and two new circuits are formed for current flow. The first circuit is composed by the self-inductance EMF of the choke L1, and the current flows through the diode of the switch S2 and the capacitor C1. The self-inductance EMF of the motor armature winding forms the second circuit, and the current flows through the same diode of the switch S2. In this state, the stored intermediate energy is recharged – the choke L1 charges the capacitor C1.

To develop a motor armature current control system, i.e. motor electromagnetic torque control, a mathematical model of the electromagnetic part of the electric drive system must be created. The model was built considering the peculiarities of the Zeta DC-DC converter integrated with the motor armature winding based on the first and second
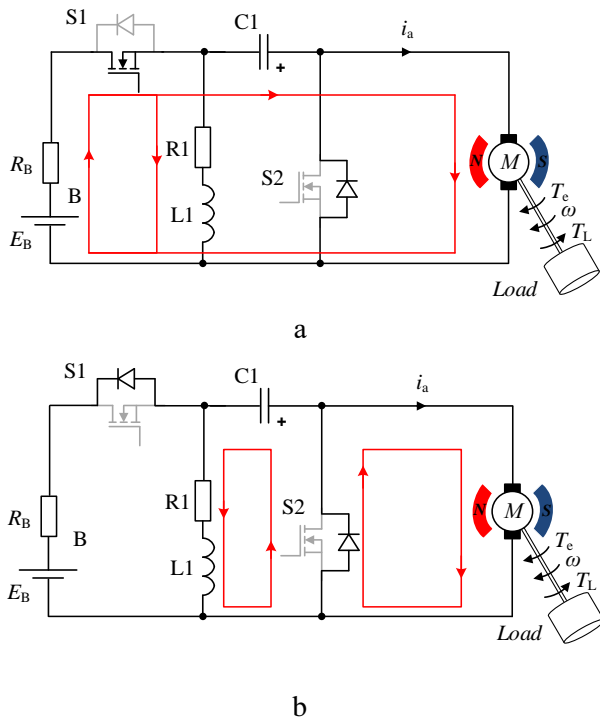
a

b

Fig. 2. DC drive in the traction mode with the Zeta DC-DC converter in the ON (a) and OFF (b) states of the switch S1
Source: compiled by the authors

Kirchhoff's laws. The model comprises three differential equations, one for each state variable that determines the energy stored in three intermediate energy storage devices: the choke L1 with inductance L_1, the capacitor C1 with capacitance C_1, and the motor armature winding with inductance L_a. The impact of each voltage or current element on the right-hand side of the equations, which is determining by the state of the switch S1, is described by its PWM duty ratio μ_1 when S1 is on and $(1-\mu_1)$ when S1 is off. The sign before each term on the right-hand side of the equation indicates its influence on the direction of change of the state variable.

The equation of torque equilibrium on the motor shaft, based on Newton's laws, yields the following fourth-order nonlinear system of differential equations:

$$
\begin{cases}
\dfrac{d}{dt}i_{L1} = \dfrac{1}{L_1}\left[(1-\mu_1)v_{C1} + \mu_1 v_B - i_{L1}R_1\right] \\[2mm]
\dfrac{d}{dt}i_a = \dfrac{1}{L_a}\left[\mu_1 v_{C1} - k_e\omega + \mu_1 v_B - i_a R_a\right] \\[2mm]
\dfrac{d}{dt}v_{C1} = \dfrac{1}{C_1}\left[(1-\mu_1)i_{L1} - \mu_1 i_a\right] \\[2mm]
\dfrac{d}{dt}\omega = \dfrac{1}{J}\left[k_e i_a - T_L\right]
\end{cases}, \quad (5)
$$

where i and v are the currents and voltages of the corresponding circuit elements, and $v_B = E_B - i_{L1}R_B$ is the battery voltage.

The DC drive in the regenerative braking mode with the SEPIC DC-DC converter

During regenerative braking mode, the SEPIC DC-DC converter transfers energy from the DC motor to the battery. The converter is controlled by the S2 switch in this mode.

When the S2 switch is turned on (see Fig. 3a), current flows through two circuits. The first circuit is composed by the capacitor C1, the switch S2, and the choke L1. In this circuit, the energy stored in the capacitor C1 charges the choke L1. The second circuit is formed by closing the back-EMF of the motor through the switch S2.

When the S2 switch is turned off (see Fig. 3b), two new parallel circuits are formed. The back-EMF of the motor forms the larger circuit, and current flows through the capacitor C1 and the switch S1 diode to the battery B. The small circuit is formed by the self-inductance EMF of the choke L1, and current flows through the same diode to the battery. During this state of operation, the energy from the motor and energy stored in the choke L1 charge the battery B. Additionally, the capacitor C1 is charged by the back-EMF of the motor too.
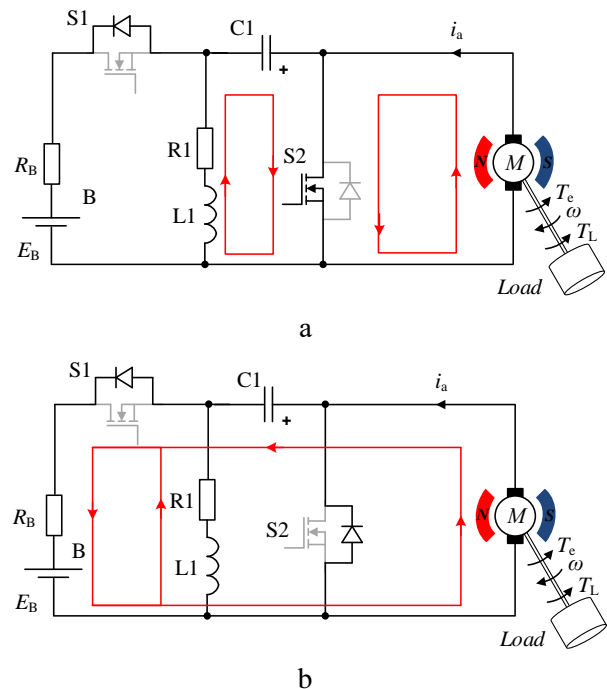

a

b

Fig. 3. DC drive in the regenerative braking mode with the SEPIC DC-DC converter during the ON (a) and OFF (b) states of the S2 switch
Source: compiled by the authors

Following the description of the operating processes of the SEPIC DC-DC converter, a mathematical model of the electromagnetic and electromechanical parts of the drive system was obtained in the form of a system of fourth-order differential equations for each of the state variables:

$$
\begin{cases}
\dfrac{d}{dt}i_{L1} = \dfrac{1}{L_1}\left[\mu_2 v_{C1} - (1-\mu_2)v_B - i_{L1}R_1\right] \\[2mm]
\dfrac{d}{dt}i_a = \dfrac{1}{L_a}\left[(1-\mu_2)(-v_B - v_{C1}) - i_a R_a + k_e \omega\right] \\[2mm]
\dfrac{d}{dt}v_{C1} = \dfrac{1}{C_1}\left[-\mu_2 i_{L1} + (1-\mu_2)i_a\right] \\[2mm]
\dfrac{d}{dt}\omega = \dfrac{1}{J}\left[-k_e i_a - T_L\right]
\end{cases}, \quad (6)
$$

where μ_2 is the PWM duty ratio of the switch S2.

MATHEMATICAL MODELING OF THE DC DRIVE AS PORT-CONTROLLED HAMILTONIAN SUBSYSTEMS

The traction mode with the Zeta DC-DC converter

Considering (1) and (5), the state vector, the diagonal inertia matrix and the vector of input variables of the subsystem in traction mode are as follows:

$$
\mathbf{x} = \begin{bmatrix} i_{L1} & i_a & v_{C1} & \omega \end{bmatrix}^\mathrm{T}, \quad (7)
$$

$$
\mathbf{D} = \mathrm{diag}\begin{bmatrix} L_1 & L_a & C_1 & J \end{bmatrix}, \quad (8)
$$

$$
\mathbf{u} = \begin{bmatrix} \mu_1 v_B & \mu_1 v_B & 0 & -T_L \end{bmatrix}^\mathrm{T}. \quad (9)
$$

Taking into account (7) and (8), the Hamiltonian function of the subsystem is described by the following expression:

$$
H(\mathbf{x}) = \frac{1}{2}\mathbf{x}^\mathrm{T}\mathbf{D}\mathbf{x} = \\
= \frac{1}{2}\left(L_1 i_{L1}{}^2 + L_a i_a{}^2 + C_1 v_{C1}{}^2 + J\omega^2\right). \quad (10)
$$

The vector of Hamiltonian partial derivatives for each of the subsystem state vector variables, considering (10), is given by:

$$
\nabla H(\mathbf{x}) = \frac{\partial H(\mathbf{x})}{\partial \mathbf{x}} = \\
= \begin{bmatrix} L_1 i_{L1} & L_a i_a & C_1 v_{C1} & J\omega \end{bmatrix}^\mathrm{T}. \quad (11)
$$

Based on (1), (5), and (7)-(11), the interconnection matrix, the damping matrix, and the port matrix of the subsystem are described by the following expressions:

$$
\mathbf{J}(\mu) = \begin{bmatrix}
0 & 0 & (\mu_1 - 1) & 0 \\
0 & 0 & \mu_1 & -k_e \\
-(\mu_1 - 1) & -\mu_1 & 0 & 0 \\
0 & k_e & 0 & 0
\end{bmatrix}, \quad (12)
$$

$$
\mathbf{R} = \mathrm{diag}\begin{bmatrix} -R_1 & -R_a & 0 & 0 \end{bmatrix}, \quad (13)
$$

$$
\mathbf{G} = \mathbf{I}. \quad (14)
$$

The regenerative braking mode with the SEPIC DC-DC converter

Based on (1) and (6), the following vectors and the inertia matrix were formed for the PCH subsystem, which refer to the braking mode of the electric drive:

$$
\mathbf{x} = \begin{bmatrix} i_{L1} & i_a & v_{C1} & \omega \end{bmatrix}^\mathrm{T}, \quad (15)
$$

$$
\mathbf{D} = \mathrm{diag}\begin{bmatrix} L_1 & L_a & C_1 & J \end{bmatrix}, \quad (16)
$$

$$
\mathbf{u} = \begin{bmatrix} -(1-\mu_2)v_B & -(1-\mu_2)v_B & 0 & T_L \end{bmatrix}^\mathrm{T}. \quad (17)
$$

The Hamiltonian function and its partial derivatives for the subsystem are as follows:

$$
H(\mathbf{x}) = \frac{1}{2}\mathbf{x}^\mathrm{T}\mathbf{D}\mathbf{x} = \\
= \frac{1}{2}\left(L_1 i_{L1}{}^2 + L_a i_a{}^2 + C_1 v_{C1}{}^2 + J\omega^2\right), \quad (18)
$$

$$
\nabla H(\mathbf{x}) = \frac{\partial H(\mathbf{x})}{\partial \mathbf{x}} = \\
= \begin{bmatrix} L_1 i_{L1} & L_a i_a & C_1 v_{C1} & J\omega \end{bmatrix}^\mathrm{T}. \quad (19)
$$

The structure matrices of the PCH subsystem are obtained by considering (1), (6) and (15)-(19):

$$
\mathbf{J}(\mu) = \begin{bmatrix}
0 & 0 & \mu_2 & 0 \\
0 & 0 & -(\mu_2 - 1) & k_e \\
-\mu_2 & (\mu_2 - 1) & 0 & 0 \\
0 & -k_e & 0 & 0
\end{bmatrix}, \quad (20)
$$

$$
\mathbf{R} = \mathrm{diag}\begin{bmatrix} -R_1 & -R_a & 0 & 0 \end{bmatrix}, \quad (21)
$$

$$
\mathbf{G} = \mathbf{I}. \quad (22)
$$

SYNTHESIS OF THE PBC SUBSYSTEMS

For the synthesis of the PBC subsystems of the LEV electric motor speed control, the following vectors of steady-state values of the state variables were formed as:

$$\bar{\mathbf{x}} = \begin{bmatrix} i_{L10} & i_{a0} & v_{C10} & \omega^* \end{bmatrix}, \qquad (23)$$

where ω^* is the reference value of the angular velocity that is set at the input of the control system.

In equation (23), the index '0' represents the steady-state values of the state variables resulting from the structural synthesis of the PBC subsystems. The PWM duty ratios μ_1 and μ_2, along with i_{L10}, i_{a0} and v_{C10}, are the fourth solutions of vector-matrix equations and reflect the structures of the CIFs synthesized for respective PBC subsystems of the traction and braking modes.

The synthesis resulted in a set of CIFs structures for the traction and braking modes of the electric drive, as shown in Table 1.

To control the S1 Zeta switch of the DC-DC converter in the traction mode of the drive, the basic structure of the CIF (without introducing additional interconnections and damping) is obtained as follows:

$$\mu_1 = \frac{k_e^2 \omega^* + R_a T_L}{k_e v_B + k_e^2 \omega^* + R_a T_L} . \qquad (24)$$

The obtained structures of the CIFs for various additional interconnections introduced in the PBC subsystem for the Zeta DC-DC converter are shown in Table 1 on the left side. The additional interconnection j_{14} has no realization, and j_{24} one forms a structure that is difficult to implement. From the four possible additional damping elements, only r_{22} and r_{44} ones are useful in forming CIFs structures. The damping r_{11} has no implementation, and r_{33} one forms the same to (24) CIF structure.

The basic structure of the CIF for controlling the S2 switch of the SEPIC DC-DC converter in the braking mode of the drive is obtained as follows:

$$\mu_2 = \frac{k_e v_B}{k_e v_B + k_e^2 \omega^* + R_a T_L} . \qquad (25)$$

The obtained CIFs structures for various additional interconnections in the PBC subsystem for the Zeta DC-DC converter are shown in Table 1 on the right side. The additional interconnections j_{14} and j_{24}, as well as the additional damping r_{11}, r_{22}, r_{33}, and r_{44}, behaved similarly to the previous case.

Table 1. **Obtained structures of the CIFs with various additional interconnections and damping for the PBC subsystems of DC motor speed control in the traction and braking modes**

	Zeta DC-DC converter (traction mode)		SEPIC DC-DC converter (braking mode)	
j_{12}	$\mu_1 = \dfrac{k_e^2 \omega^* + R_a T_L - j_{12} i_{L1} k_e}{k_e v_B + k_e^2 \omega^* + R_a T_L - j_{12} k_e (i_{L1} + i_a)}$	(26)	$\mu_2 = \dfrac{k_e v_B + j_{12} i_a k_e}{k_e v_B + k_e^2 \omega^* + R_a T_L + j_{12} k_e (i_{L1} + i_a)}$	(32)
j_{13}	$\mu_1 = \dfrac{(k_e^2 \omega^* + R_a T_L)(1 - j_{13})}{k_e v_B (1 - j_{13}) + k_e^2 \omega^* + R_a T_L - j_{13} k_e v_{C1}}$	(27)	$\mu_2 = -\dfrac{j_{13}(k_e^2 \omega^* - R_a T_L - k_e v_{C1} + R_a T) - k_e v_B}{k_e v_B (1 + j_{13}) + k_e^2 \omega^* + R_a T_L + j_{13} k_e v_{C1}}$	(33)
j_{23}	$\mu_1 = \dfrac{k_e^2 \omega^* + R_a T_L + j_{23} k_e v_{C1}}{k_e v_B + k_e^2 \omega^* + R_a T_L + j_{23} k_e (v_{C1} + v_B)}$	(28)	$\mu_2 = \dfrac{k_e v_B (1 - j_{23})}{k_e v_B + k_e^2 \omega^* + R_a T_L - j_{23} k_e (v_{C1} + v_B)}$	(34)
j_{34}	$\mu_1 = \dfrac{k_e^2 \omega^* + R_a T_L - j_{34} R_a v_{C1}}{k_e v_B + k_e^2 \omega^* + R_a T_L - j_{34} R_a (v_{C1} + v_B)}$	(29)	$\mu_2 = \dfrac{v_B (k_e - j_{34} R_a)}{k_e v_B + k_e^2 \omega^* + R_a T_L - j_{34} R_a (v_{C1} + v_B)}$	(35)
r_{22}	$\mu_1 = \dfrac{k_e^2 \omega^* + R_a T_L + r_{22}(T_L - k_e i_a)}{k_e v_B + k_e^2 \omega^* + R_a T_L + r_{22}(T_L - k_e i_a)}$	(30)	$\mu_2 = \dfrac{k_e v_B}{k_e v_B + k_e^2 \omega^* + R_a T_L + r_{22}(T_L + k_e i_a)}$	(36)
r_{44}	$\mu_1 = \dfrac{k_e^2 \omega^* + R_a T_L - r_{44} R_a (\omega - \omega^*)}{k_e v_B + k_e^2 \omega^* + R_a T_L - r_{44} R_a (\omega - \omega^*)}$	(31)	$\mu_2 = \dfrac{k_e v_B}{k_e v_B + k_e^2 \omega^* + R_a T_L - r_{44} R_a (\omega - \omega^*)}$	(37)

Source: **compiled by the authors**

CONTROL SYSTEM DESIGN

The functional diagram of the investigated DC drive system with the Zeta-SEPIC DC-DC converter and synthesized PBC motor speed system is shown in Fig. 4.

Four sensors were used for implementation of the control system. Three of them, the battery voltage sensor BVS, the motor speed sensor SS, and the load torque sensor TS, are used to generate the PWM duty ratios to control the S1 and S2 switches. The fourth motor armature current sensor CS is used as a control signal for the switch S_m, which provides the function of switching the drive operating mode and, accordingly, the type of DC-DC converter in operation. The input reference signal is ω^*.

The technical implementation of these sensors can be carried out in well-known ways, for example: the BVS and CS sensors should be the best chosen from those operating on the Hall Effect; the SS can as an incremental encoder, the TS can be implemented as a torque observer, which structure and parameters can be obtained by known methods.
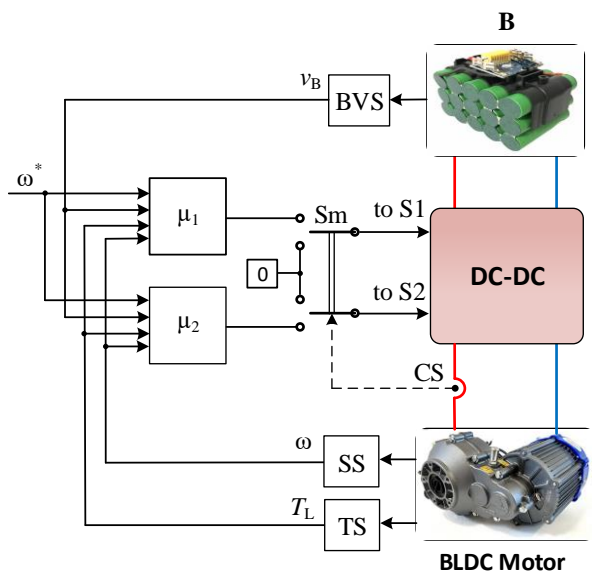

Fig. 4. Functional diagram of the investigated electric drive with PBC speed control system of DC motor
Source: **compiled by the authors**

However, when such passivity-based drive speed control system is used, the problem arises of providing a motor armature current limitation in transient modes and drive overload. To solve this problem, it is proposed to use an auxiliary speed control subsystem as shown in Fig. 5. This subsys-tem follows the principle of subordinate coordinate control utilizing an external angular speed control loop with a PI speed controller SC and two internal armature current control subsystems, respectively for the traction and braking modes of the drive. The last subsystems are implemented as passivity-based current control subsystems μ_{12} and μ_{22}, which are synthesized similarly to the main passivity-based speed control subsystems μ_{11} and μ_{21} using the IDA method.

The best expressions of the CIFs for the pas-sivity-based current control subsystems were obtained in [26] as:

$$\mu_{12} = \frac{k_e \omega + R_a i_a^* - r_{22}(i_a - i_a^*)}{v_B + k_e \omega + R_a i_a^* - r_{22}(i_a - i_a^*)}, \qquad (38)$$

$$\mu_{22} = \frac{v_B}{v_B + k_e \omega - R_a i_a^* + r_{22}(i_a - i_a^*)}. \qquad (39)$$

where i_a^* represents the reference value of the motor armature current generated at the output of the speed controller.

It is important to note that this implementation of current limitation does not require the use of additional coordinate sensors that avoids any complications to the existing control system. The control transition to current limiting is provided through an additional switch S_{m3}. This switch transfers control from the main passivity-based speed control system to the auxiliary one when the armature current reaches the set current limiting value.

RESEARCH OF THE OBTAINED STRUCTURES OF CIFS BY COMPUTER SIMULATION

The study was performed using the Zeta-SEPIC DC-DC converter with the same parameters as in [12]: a maximum power of 600 W, a supply voltage of 24 V, a rated output voltage of 48 V. The value of the PWM carrier frequency was chosen of 20.0 kHz. The experimental DC motor had a rated power of 300 W, a supply voltage of 48 V, and a rotational speed of 1000 rpm. Other its parameters were as follows: an armature winding resistance of 0.45 Ohm, an armature inductance of 0.02 H, and the motor constant $k_e = 0.3737$ V·s. The drive's moment of inertia was 0.05 kg·m². A computer model was created in the Matlab/Simulink environment (Fig. 6) based on the power scheme shown in Fig. 1b and the functional diagram presented in Fig. 5.
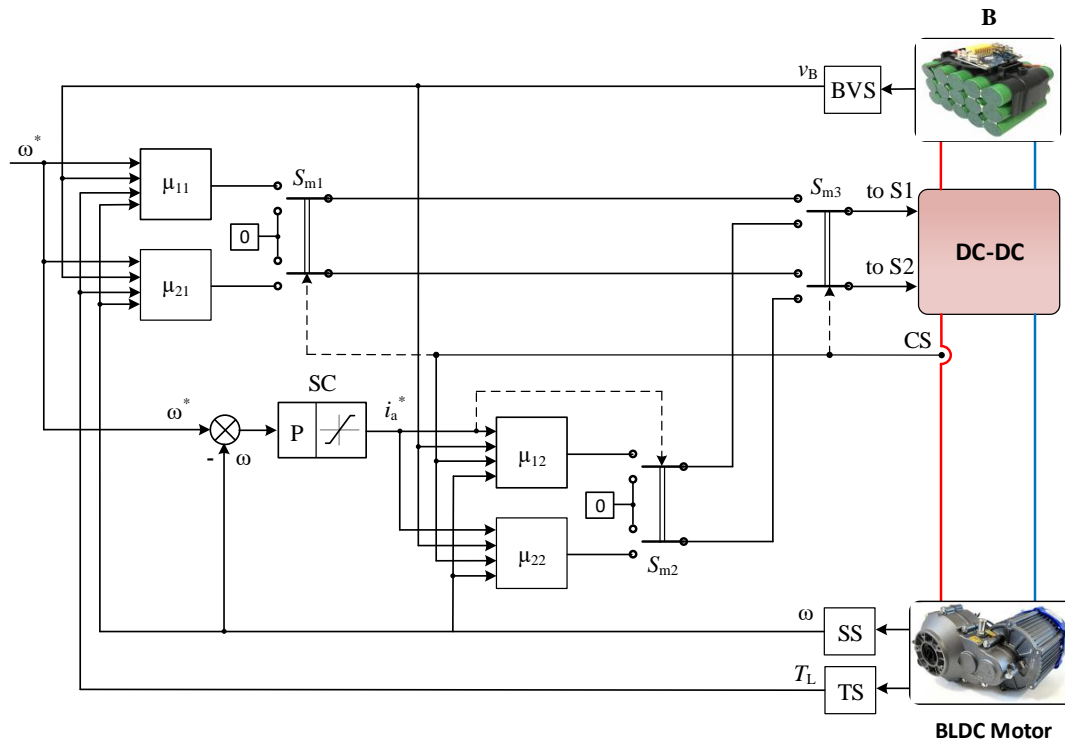
Fig. 5. Functional diagram of the electric drive with PBC motor speed control system and PBC armature current limiting subsystem
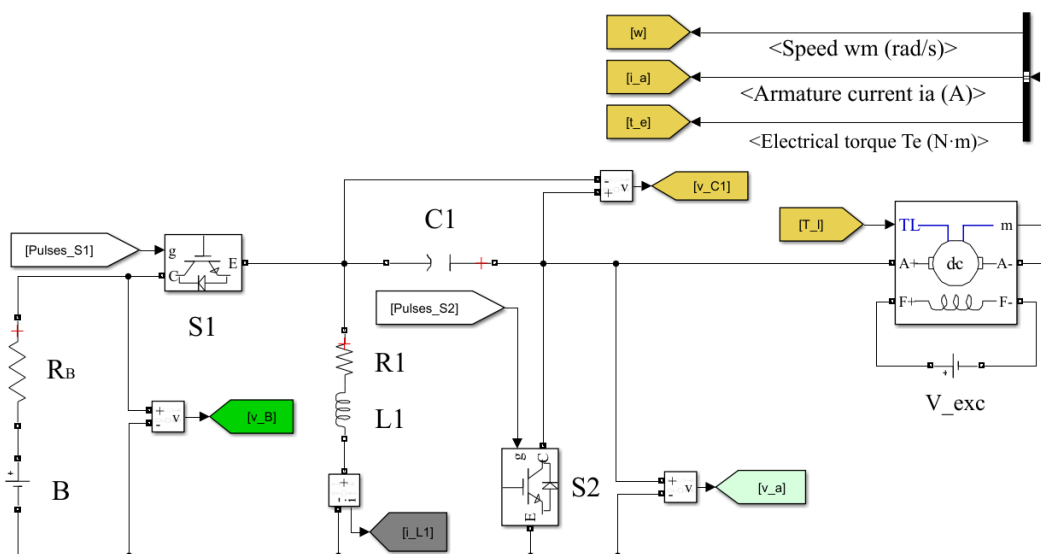*Source:* compiled by the authors

Fig. 6. Computer model of the power part of the studied electric drive system
Source: compiled by the authors

The studies of the obtained CIF structures presented in Table 1 showed an increase in the fluctuations of the system main variables compared to the basic structures (24) and (25). This is because the PBC system with CIFs (26)-(37) becomes closed due to the introduced interconnections. The conducted research shown that introduction an additional damping r_{44} resulted in the best performance in

terms of ensuring control quality and moderate system fluctuations. Through the research, it was determined that the most effective is the CIF structure (31) for the traction mode and the CIF structure (37) for the regenerative braking mode of drive. The control subsystems synthesized by PBC effectively controlled the drive speed for both traction and braking modes of motor operation. The use of CIF structures

(31) for the Zeta converter and (37) for the SEPIC converter ensures minimal fluctuations in the motor armature current and, consequently, in the electromagnetic torque.

However, computer studies revealed different drive dynamics at different angular velocities of the motor due to the nonlinearity of the DC-DC converters. To eliminate this drawback, the damping coefficient r_{44} was adapted to the value of the angular velocity.

The optimal dependencies of the damping coefficient r_{44} on the motor angular velocity resulting from computer studies are as follows:

- for the traction mode

$$r_{44}(\omega) = -0.298367 - 0.000220824\omega + \\ +3.08858 \cdot 10^{-6}\omega^2 - 7.38151 \cdot 10^{-8}\omega^3; \quad (40)$$

- for the regenerative braking mode

$$r_{44}(\omega) = -0.456452 - 0.000359921\omega + \\ +2.45563 \cdot 10^{-5}\omega^2 - 4.0404 \cdot 10^{-8}\omega^3. \quad (41)$$

According to the research results, for the range of changes in the motor angular velocity from zero to 100 rad/s, the values of the damping coefficient r_{44} according to expressions (40) and (41) vary from -0.3 to -0.3585 in the CIF structure (31) for the drive's traction mode and from -0.32 to -0.46 in the CIF structure (37) in the braking mode. The results of this adaptation are shown in Fig. 7 for the traction mode and in Fig. 8 for the regenerative braking mode.
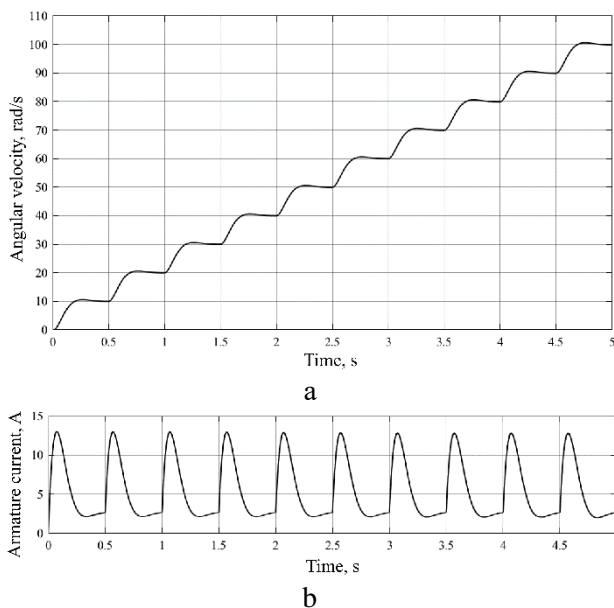

Fig. 7. **Time diagrams of the angular velocity (a) and armature current (b) of the motor operating in the traction mode with a step increase in the reference speed**
Source: **compiled by the authors**

A gradual change of 10 rad/s was set in the directions of increasing and decreasing of the angular velocity, respectively, at constant value of a load torque of 1.0 N·m. The obtained time diagrams demonstrate almost identical dynamics of the drive operation in the entire range of its speed control ensuring high accuracy of its control with a slight overshoot.
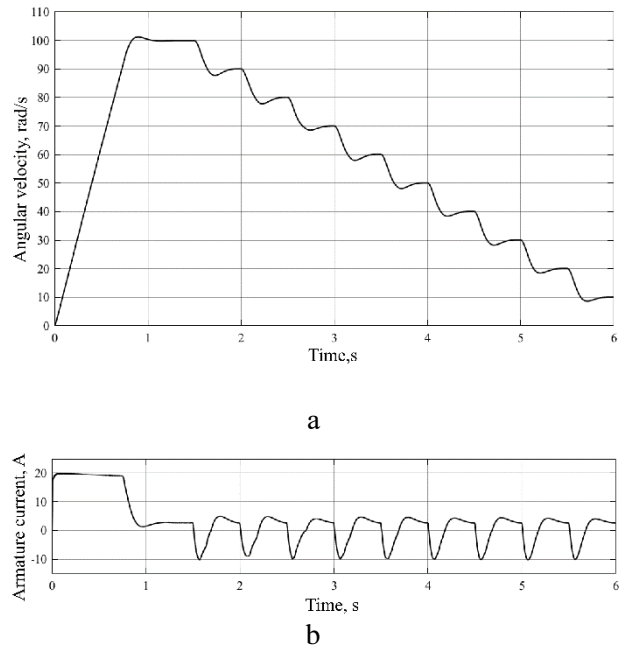

Fig. 8. **Time diagrams of the angular velocity (a) and armature current (b) of the motor operating in the braking mode with a step decrease in the reference speed**
Source: **compiled by the authors**

Fig. 9 shows the results of simulation studies of the PBC motor speed control system. The study followed the set angular velocity of the drive motion (Fig. 9a), which includes low and high-speed operation sections with motor acceleration and braking modes, as well as a burst load in the time interval of 3.0-3.5 seconds. The results indicate a good working out of the reference speed signal by the drive (Fig. 9a) with a slight overshoot and almost no steady-state error. Fig. 9b shows the motor armature voltage with a pulsed nature with PWM carrier frequency. It is important to note that the PBC subsystems of the armature current control fully ensure the drive's operation under current limitation. The motor armature current is limited at the set values: 20 A for the traction mode and at -15 A for the braking mode of the drive, as shown in Fig. 9c. The electromagnetic torque time diagram in Fig. 9d fully reproduces the shape of the current time diagram. The battery current (Fig. 9e) follows the shape of the power consumed from the battery. The time diagram shows

that braking power recovery is inefficient at low drive speeds (0.75-1.0 s). However, braking at max- imum speed (4.0-4.4 s) provides a battery charging current of -20 to -10 A.
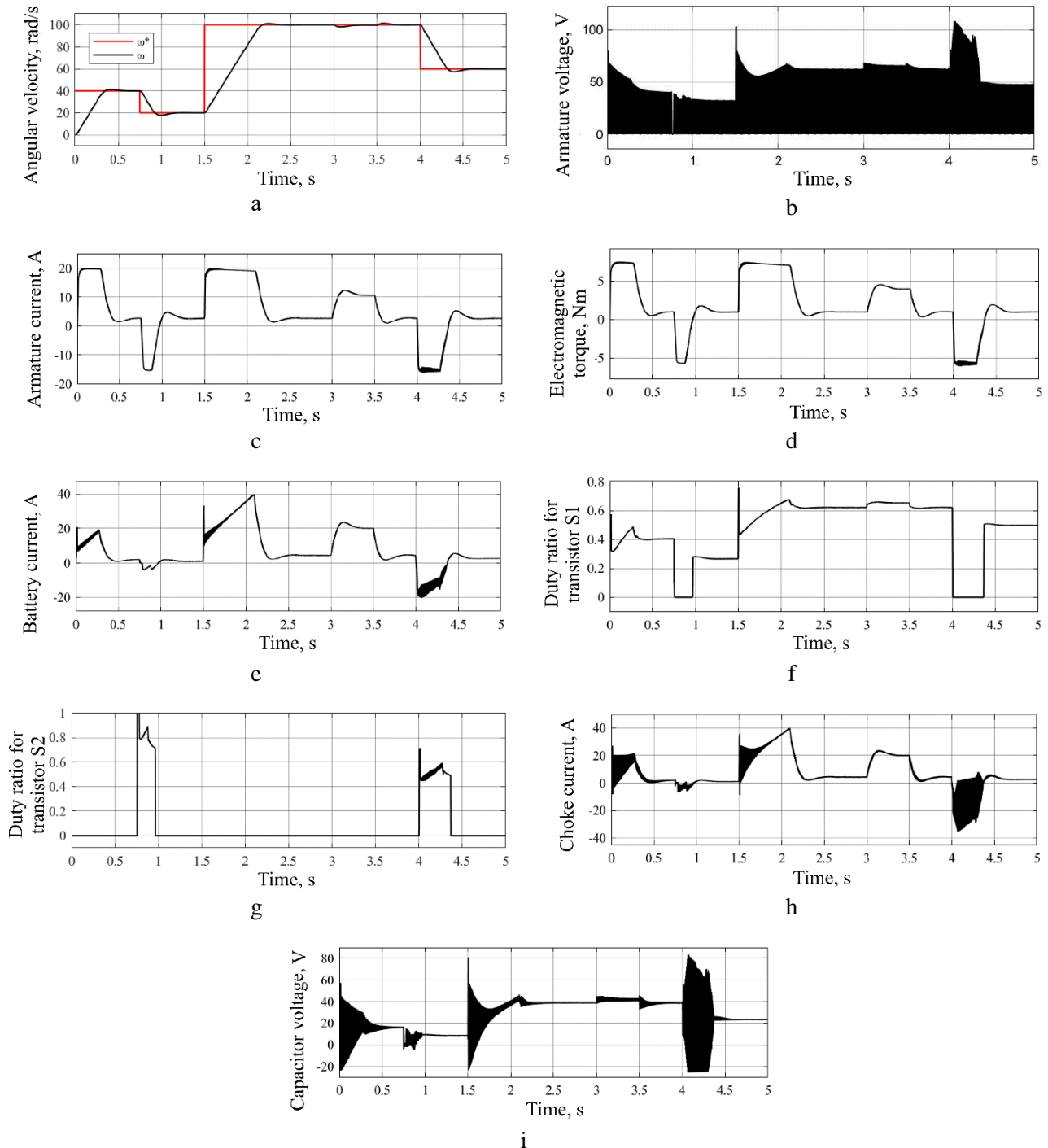

Fig. 9. **Time diagrams of the main variables of the electric drive system obtained as a result of comput-er simulation:**
a – angular velocity; b – armature voltage;
c – armature current; d – electromagnetic torque; e – battery current; f – duty ratio for the switch S1;
g – duty ratio for the switch S2;
h – choke current; i – capacitor voltage
Source: **compiled by the authors**

The time diagrams of the duty ratio of the control signals for the switch S1 (Fig. 7f) and for the switch S2 (Fig. 9g) show the sequence of their operation. By comparing these curves with the battery current time diagram (Fig. 9e), it is possible to determine the correspondence to the drive operating modes. Specifically, the switch S1 operates in traction mode and the switch S2 operates in braking mode. The time diagrams of the current of the choke L1 (Fig. 9h) and the voltage across the capacitor C1 (Fig. 9i) exhibit significant pulsations, especially during transient modes of the drive. This is due to the peculiarity of the Zeta-SEPIC DC-DC converter.

CONCLUSIONS

The considered LEV electric drive system is characterized by a low battery voltage, but the use of the Zeta-SEPIC DC-DC converter with buck-boos properties ensured that the motor supply voltage could be adjusted from zero to a nominal value that is twice the battery voltage.

The use of mode decomposition in the synthesis of the passivity-based DC motor speed control system integrated in the Zeta-SEPIC DC-DC converter, which is a rather complex and nonlinear control object, made it possible to simplify the task of synthesizing the control system and to ensure the high quality of the obtained static and dynamic characteristics of the drive.

The desired PBC structures were formed to allow a flexible debugging of the subsystem implementation of various structures and adaptations of interconnections and damping to achieve the required effects on the subsystems. The mode decomposition was utilized to prevent mutual influence between the subsystems. The CIFs for two subsystems of motor speed control in the traction and regenerative braking modes, as well as two subsystems of motor armature current control in current limiting modes, have simple synthesized structures. The laws of adaptation of the damping coefficient to the angular velocity of the motor ensure the same and independent dynamics of the electric drive at all speeds.

The simulation studies confirmed the effectiveness of the control system developed by PBC for the LEV electric drive system, which is a rather complex nonlinear object, at different speeds and loads.

REFERENCES

1. "Electric Vehicles – Worldwide". – Available from: https://www.statista.com/outlook/mmo/electric-vehicles/worldwide. – [Accessed: Feb. 2023].

2. Andwari, A. M., Pesiridis, A., Rajoo, S., Martinez-Botas, R. & Esfahanian, V. "A review of battery electric vehicle technology and readiness levels". *Renewable and Sustainable Energy Reviews*. 2017; 78: 414–430, https://www.scopus.com/authid/detail.uri?authorId=57293009000. DOI: https://doi.org/10.1016/j.rser.2017.03.138.

3. Mesimäki, J. & Lehtonen, E. "Light electric vehicles: the views of users and non-users". *European Transport Research Review*. 2023; 15:33: 1–15, https://www.scopus.com/authid/detail.uri?authorId=57225037723. DOI: https://doi.org/10.1186/s12544-023-00611-3.

4. Far, M. F., Miljavec, D., Manko, R. et al. "Modular and scalable powertrain for multipurpose light electric vehicles". *World Electr. Veh. J.* 2023; 14 (309): 1–12, https://www.scopus.com/authid/detail.uri?authorId=56441434300. DOI: https://doi.org/10.3390/wevj14110309.

5. Wüstenhagen, S., Beckert, P., Lange, O. & Franze, A. "Light electric vehicles for muscle–battery electric mobility in circular economy: A comprehensive study". *Sustainability*. 2021; 13: 13793, https://www.scopus.com/authid/detail.uri?authorId=57195330211.
DOI: https://doi.org/10.3390/su132413793.

6. Jagadeesh, I. & Indragandhi, V. "Review and comparative analysis on dc-dc converters used in electric vehicle applications". *IOP Conf. Series: Materials Science and Engineering*. 2019; 623: 1–15, https://www.scopus.com/authid/detail.uri?authorId=57202745970&origin=recordpage. DOI: https://doi.org/10.1088/1757-899X/623/1/012005.

7. Reddy, K.-J. & Sudhakar, N. "Energy sources and multi-input DC-DC converters used in hybrid electric vehicle applications – A review". *Int. J of Hydrogen Energy*. 2018; 43: 17387–17408, https://www.scopus.com/authid/detail.uri?authorId=57199323238. DOI: https://doi.org/10.1016/j.ijhydene.2018.07.076.

8. Reddy, K.-S. & Sreenivasappa, B. V. "Review on power converters for electric vehicles". *J Xi'an University of Architecture & Technology*. 2020; 12(8): 82–105. Available from: http://www.xajzkjdx.cn/gallery/11-aug2020.pdf. – [Accessed: Sept. 2022].

9. Siddharthan, N. & Balasubramanian, B. "Performance evaluation of SEPIC, Luo and ZETA converter". *Int. J of Power Electronics and Drive System.* 2019; 10: 374–380, https://www.scopus.com/authid/detail.uri?authorId=57205345977.
DOI: https://doi.org/10.11591/ijpeds.v10.i1.pp374-380.

10. Tytelmaier, K., Husev, O., Veligorskyi, O. & Yershov, R. "A review of non-isolated bidirectional DC-DC converters for energy storage systems". *II Int. Young Scientists Forum on Applied Physics and Engineering (YSF-2016).* 2016. p. 22-28, https://www.scopus.com/authid/detail.uri?authorId=57188715517.
DOI: https://doi.org/10.1109/YSF.2016.7753752.

11. Ravi, D., Reddy, B. M. & Shimi, S. L. "Bidirectional dc to dc converters: an overview of various topologies, switching schemes and control techniques". *Int. J of Engineering & Technology*. 2018; 7 (4.5): 360–365, https://www.scopus.com/authid/detail.uri?authorId=57203949236. DOI: https://doi.org/10.14419/ijet.v7i4.5.20107.

12. Khan, M. A., Ahmed, A., Husain, I., Sozer, Y. & Badawy, M. "Performance analysis of bidirectional DC–DC converters for electric vehicles". *IEEE Trans. Industry Applications*. 2015; 51: 3442–3452, https://www.scopus.com/authid/detail.uri?authorId=55521299600.
DOI: https://doi.org/10.1109/TIA.2015.2388862.

13. Ruseler, A. & Barbi, I. "Isolated Zeta-SEPIC bidirectional dc-dc converter with active-clamping". *Brazilian Power Electronics Conf.* 2013. p. 123–128, https://www.scopus.com/authid/detail.uri?authorId=37104808000. DOI: https://doi.org/10.1109/COBEP.2013.6785104.

14. Lee, H.-Y., Liang, T.-J., Chen, J.-F. & Chen, K.-H. "Design and implementation of a bidirectional SEPIC-Zeta DC-DC converter". *IEEE Int. Symp. Circuits and Systems*. 2014. p. 101–104, https://www.scopus.com/authid/detail.uri?authorId=56369414000. DOI: https://doi.org/10.1109/ISCAS.2014.6865075.

15. Singh, A.-K. & Pathak, M.-K. "Single-stage ZETA-SEPIC-based multifunctional integrated converter for plug-in electric vehicles". *IET Electrical Systems in Transportation.* 2018; 8: 101–111, https://www.scopus.com/authid/detail.uri?authorId=57199212543. DOI: https://doi.org/10.1049/iet-est.2017.0063.

16. Shchur, I. "Bidirectional single-stage Zeta-SEPIC DC-AC converter for traction BLDC motors". *IEEE 3rd KhPI Week on Advanced Technology*. 2022. p. 1–6, https://www.scopus.com/authid/detail.uri?authorId=36348908300.
DOI: https://doi.org/10.1109/KhPIWeek57572.2022.9916353.

17. Arunraj, S., Murugesan, S., Nandhini, T. U. & Keerthana, K. "A novel zeta converter with pi controller for power factor correction in induction motor". *Int. J of Scientific Research in Science and Technology*. 2017; 3 (8): 230–234. Available from: https://ijsrst.com/IJSRST173845. – [Accessed: Sept. 2023].

18. Aseem, K. & Kumer, S.-S. "Closed loop control of DC-DC converters using PID and FOPID controllers". *Int. J of Power Electronics and Drive Systems*. 2020; 11: 1323–1332, https://www.scopus.com/authid/detail.uri?authorId=55991374700. DOI: https://doi.org/10.11591/ijpeds.v11.i3.pp1323-1332.

19. Henao-Bravo, E.-E., Saavedra-Montes, A.-J., Ramos-Paja, C.-A., Bastidas-Rodriguez, J.-D. & Montoya, D. G. "Charging/discharging system based on zeta/sepic converter and a sliding mode controller for dc bus voltage regulation". *IET Power Electron*. 2020; 13: 1514–1527, https://www.scopus.com/authid/detail.uri?authorId=57201861329.
DOI: https://doi.org/10.1049/iet-pel.2019.0746.

20. Ali, M.-O. & Ahmad, A.-H. "Design, modelling and simulation of controlled sepic DC-DC converter-based genetic algorithm". *Int. J of Power Electronics and Drive System*. 2020; 11: 2116–2125, https://www.scopus.com/authid/detail.uri?authorId=57218892987. DOI: https://doi.org/10.11591/ijpeds.v11.i4.pp2116-2125.

21. Ibrahim, M.-A. "Performance evaluation of PI controller for positive output Luo converter". *Int. J of Power Electronics and Drive System.* 2020; 11: 1816–1825, https://www.scopus.com/authid/detail.uri?authorId=57205021545. DOI: https://doi.org/10.11591/ijpeds.v11.i4.pp1816-1825.

22. Benmouna, A., Becherif, M., Depernet, C. & Ebrahim, M.-A. "Novel energy management technique for hybrid electric vehicle via interconnection and damping assignment passivity based control". *Renewable Energy.* 2018; 119: 116–128, https://www.scopus.com/authid/detail.uri?authorId=57191838421. DOI: https://doi.org/10.1016/j.renene.2017.11.051.

23. Shchur, I. Z. & Biletskyi, Y. O. "Improved structure of passivity-based control of battery-supercapacitor hubrid energy storage system". *Applied Aspects of Information Technology.* 2020; 3 (4): 232–245. DOI: https://doi.org/10.15276/aait.04.2020.2.

24. Biletskyi, Y. O., Shchur, I. Z. & Kuzyk, R.-I. V. "Passivity-based control system for stand-alone hybrid electrogenerating complex". *Applied Aspects of Information Technology.* 2021; 4 (2): 140–152. DOI: https://doi.org/10.15276/aait.02.2021.2.

25. Shchur, I. & Kuzyk, R.-I. "Mode decomposition passivity-based control of bidirectional Zeta–SEPIC DC-DC converter". *21th IEEE Conf. Modern Electrical and Energy Systems.* 2022. p. 1–6, https://www.scopus.com/authid/detail.uri?authorId=36348908300. DOI: https://doi.org/10.1109/MEES58014. 2022.10005701

26. Shchur, I. & Kuzyk, R.-I. "Mode decomposition passivity-based control of DC drive based on bidirectional Zeta–SEPIC DC-DC converter for electric vehicles". *XIth Int. Scientific Conf. Information Technologies in Agro-Industrial Complex.* 2022. p. 26–28. Available from: https://itea.lnup.edu.ua/resources/ITEA-2022_tezy_end.pdf. – [Accessed: Sept. 2023].

Conflicts of Interest: The authors declare that there is no conflict of interest

Режимно декомпонована система пасивного керування швидкістю DC електропривода з двонаправленим Zeta-SEPIC DC- DC перетворювачем для малих електричних транспортних засобів

Кузик Ростислав-Іван Валерійович[1]
ORCID: https://orcid.org/0000-0002-6483-2223; rostyslav-ivan.v.kuzyk@lpnu.ua
Щур Ігор Зенонович[1]
ORCID: https://orcid.org/0000-0001-7346-1463; ihor.z.shchur@lpnu.ua. Scopus Author ID: 36348908300
[1] Національний університет «Львівська політехніка», вул. С. Бандери, 12. Львів, 79013, Україна

АНОТАЦІЯ

На даний час електричні транспортні засоби малої потужності стрімко розвиваються, набираючи різних форм. Для реалізації електропривода таких засобів, які живляться від акумуляторних батарей, найпростішою системою електропривода є двигун постійного струму, керований DC-DC перетворювачем. У цій роботі застосовано двонаправлений Zeta-SEPIC DC-DC перетворювач, в який інтегровано двигун постійного струму. Така реалізація забезпечує керування швидкістю та моментом двигуна в режимах тяги та рекуперативного гальмування, а також дає змогу застосувати батарею нижчої напруги порівняно з номінальною напругою двигуна, що зменшує масу батареї та підвищує безпечність експлуатації привода. В роботі застосовано декомпозиційний підхід, зокрема синтезовано дві окремі підсистеми керування кутовою

швидкістю двигуна окремо для тягового (Zeta) та гальмівного (SEPIC) режимів роботи привода. Для синтезу підсистем в цих режимах використано метод пасивного керування, який базується на енергетичних закономірностях протікання процесів у системах та забезпечує асимптотичну стійкість нелінійних систем, у даному випадку підсистем четвертого порядку для регулювання швидкості. Окрім того, було реалізовано обмеження струму двигуна на заданому рівні з використанням синтезованих пасивних підсистем регулювання струму третього порядку. В результаті синтезу отримано набори можливих структур формувачів керуючих впливів (ФКВ) для усіх підсистем пасивного керування роботою двигуна за допомогою Zeta та SEPIC DC-DC перетворювачів. Проведено дослідження роботи отриманих структур ФКВ, відібрано найбільш дієві з них та шляхом імітаційного комп'ютерного моделювання в середовищі Matlab/Simulink визначено закони адаптації їх параметрів до величини кутової швидкості двигуна. Результати комп'ютерного симулювання показали добрі результати роботи привода в статичних та динамічних режимах роботи.

Ключові слова: малий електротранспорт; Zeta DC-DC перетворювач; SEPIC DC-DC перетворювач; DC електропривод; пасивне керування; порт-Гамільтонова система; метод призначення взаємозв'язків та демпфувань

ABOUT THE AUTHORS

Rostyslav-Ivan V. Kuzyk - post graduate student of the Department of the Electric Mechatronics and Computerized Electromechanical Systems. Lviv Polytechnic National University, 12, S. Bandera Str. Lviv, 79013, Ukraine
ORCID: https://orcid.org/0000-0002-6483-2223; rostyslav-ivan.v.kuzyk@lpnu.ua
Research field: Nonlinear control theory; energy-based control system synthesis; renewable energy sources

Кузик Ростислав-Іван Валерійович - аспірант кафедри Електромехатроніки і комп'ютеризованих електромеханічних систем. Національний університет «Львівська політехніка», вул. С. Бандери, 12. Львів, 73013, Україна

Ihor Z. Shchur - Doctor of Engineering Sciences, Professor, Head of the Department of the Electric Mechatronics and Computerized Electromechanical Systems. Lviv Polytechnic National University, 12, S. Bandera Str. Lviv, 79013, Ukraine
ORCID: https://orcid.org/0000-0001-7346-1463; ihor.z.shchur@lpnu.ua. Scopus Author ID: 36348908300
Research field: Control systems of vehicle electric drive; renewable energy, energy storage systems; energy-based mathematical modeling and synthesis of control systems

Щур Ігор Зенонович - доктор технічних наук, професор, зав. каф. Електромехатроніки і комп'ютеризованих електромеханічних систем. Національний університет «Львівська політехніка», вул. С. Бандери, 12. Львів, 73013, Україна